NACA TN 3356
9644
TECH LIBRARY KAFB, NM
0066182

NATIONAL ADVISORY COMMITTEE FOR AERONAUTICS

TECHNICAL NOTE 3356

EFFECT OF LAG OF SIDEWASH ON THE VERTICAL-TAIL CONTRIBUTION TO OSCILLATORY DAMPING IN YAW OF AIRPLANE MODELS

By Lewis R. Fisher and Herman S. Fletcher

Langley Aeronautical Laboratory
Langley Field, Va.

Washington
January 1955

AFMDC
TECHNICAL LIBRARY
AFL 2611

1Z

TECH LIBRARY KAFB, NM
0066182

NATIONAL ADVISORY COMMITTEE FOR AERONAUTICS

TECHNICAL NOTE 3356

EFFECT OF LAG OF SIDEWASH ON THE VERTICAL-TAIL CONTRIBUTION TO OSCILLATORY DAMPING IN YAW OF AIRPLANE MODELS

By Lewis R. Fisher and Herman S. Fletcher

SUMMARY

Two models were tested for which the rate of change of sidewash with angle of sideslip could be varied. For the first model, this effect was obtained by mounting auxiliary vertical fins on the fuselage at the assumed center of gravity; for the second model, the change in the gradient of the sidewash was accomplished by varying the vertical position of the wing. In effect, these models permitted a systematic variation of the sidewash gradient at the vertical tail.

Both models were tested in steady-yawing flow and by the freely damped oscillation-in-yaw technique to establish the effect of the lag of the sidewash on the unsteady lateral damping of these models.

An analysis indicated that the oscillatory damping in yaw is proportional to a factor which depends on the lag of the sidewash whereas the steady-state damping is independent of the lag of the sidewash. Secondly, the directional stability is influenced by the static sidewash under both steady- and oscillatory-flow conditions but is not affected by the lag of the sidewash. The experimental results of this investigation verified qualitatively these analytically predicted trends. No consistent effect of frequency on the oscillatory damping in yaw was evident in the frequency range covered by this investigation.

A 45° sweptback-wing model at an angle of attack of 16° exhibited values of the oscillatory damping in yaw which were much larger than corresponding values of the steady-state damping in yaw. This increase in damping is believed to be the contribution of the wing itself to the yawing moment due to sideslipping acceleration.

INTRODUCTION

The poor damping of the lateral oscillation encountered in the flight behavior of some present-day airplanes has led to renewed consideration of

several means for improving the lateral damping of airplanes. One such method would take advantage of the lag of the sidewash at the vertical tail arising from a vortex generator on the fuselage upstream of the tail surfaces. The wing of the airplane, for example, is one such vortex generator. Other examples could logically be a canard-type surface, a radome, or possibly a cockpit canopy.

The lag of the sidewash at the vertical tail and its effect upon the damping in yaw of the tail is entirely analogous to the lag of the downwash and its effect on the damping in pitch of a horizontal tail which was first discussed by Cowley and Glauert in reference 1. The lag of the downwash was treated, by Cowley and Glauert, as an additional angle of attack of the horizontal tail which was due to the time required for the wing disturbance to travel the distance between the wing and the horizontal tail. A refinement of this concept was introduced by Jones and Fehlner (ref. 2) who additionally considered, in an approximate manner, the variations in the vertical velocities at the tail due to the varying wing wake and the lag in the development of lift at the horizontal tail.

The purpose of this investigation was to vary the rate of change of sidewash with angle of sideslip $\frac{\partial \sigma}{\partial \beta}$ for several airplane models and to measure the resulting effects on the damping in yaw in a steady wind flow and by freely damped oscillation tests. From analogy to the pitching case, the lateral damping due to the vertical tail during oscillation in yaw might be expected to be increased by approximately the factor $1 - \frac{\partial \sigma}{\partial \beta}$ over the damping due to steady yawing. The slope $\frac{\partial \sigma}{\partial \beta}$ was varied by (1) the use of auxiliary vertical fins mounted on the fuselage at the assumed center of gravity of a fuselage—vertical-tail model, and (2) variation of the wing height of two models with aspect-ratio-4 wings which were swept back 0° and 45°. The former method has some semblance to the use of canard-type surfaces on an airplane or missile whereas the latter method is an alternate means for controlling the sidewash, as well as the downwash, at the tail surfaces.

SYMBOLS

The data are referred to the system of stability axes and are presented in the form of standard NACA coefficients of forces and moments about the quarter-chord point of the mean aerodynamic chord of the normal wing location of the model tested. (See fig. 1.) The coefficients and symbols used herein are defined as follows:

A aspect ratio, $\frac{b^2}{S}$

b span, ft

C_l rolling-moment coefficient, $\frac{L'}{qS_w b_w}$

$C_{l_\beta} = \frac{\partial C_l}{\partial \beta}$

$C_{l_{\dot{\beta}}} = \frac{\partial C_l}{\partial\left(\frac{\dot{\beta} b}{2V}\right)}$

$C_{l_r} = \frac{\partial C_l}{\partial\left(\frac{rb}{2V}\right)}$

C_n yawing-moment coefficient, $\frac{N}{qS_w b_w}$

$C_{n_\beta} = \frac{\partial C_n}{\partial \beta}$

$C_{n_{\dot{\beta}}} = \frac{\partial C_n}{\partial\left(\frac{\dot{\beta} b}{2V}\right)}$

$C_{n_r} = \frac{\partial C_n}{\partial\left(\frac{rb}{2V}\right)}$

$C_{n_{\dot{r}}} = \frac{\partial C_n}{\partial\left(\frac{\dot{r} b^2}{4V^2}\right)}$

C_Y lateral-force coefficient, $\frac{Y}{qS_w}$

$C_{Y_\beta} = \frac{\partial C_Y}{\partial \beta}$

$C_{Y_{\dot{\beta}}} = \dfrac{\partial C_Y}{\partial\left(\dfrac{\dot{\beta}b}{2V}\right)}$

$C_{Y_r} = \dfrac{\partial C_Y}{\partial\left(\dfrac{rb}{2V}\right)}$

c	chord, ft
$\bar{c}$	mean aerodynamic chord, ft
c_t	mean chord of vertical tail, $\dfrac{c_{root} + c_{tip}}{2}$, ft
F_1, F_2, F_3	designations of auxiliary fins of three different aspect ratios
f	frequency, cps
I_Z	yawing moment of inertia, slug-ft^2
k	reduced-frequency parameter referred to semichord of vertical tail, $\dfrac{\omega c_t}{2V}$
L'	rolling moment, ft-lb
l_t	distance from origin of axes to quarter-chord point of vertical tail, ft
N	yawing moment, ft-lb
N_ψ	mechanical spring constant, ft-lb/radian
q	dynamic pressure, $\frac{1}{2}\rho V^2$, lb/sq ft
r, $\dot{\psi}$	yawing velocity, $\dfrac{\partial\psi}{\partial t}$, radians/sec
$\dot{r}$	yawing acceleration, $\dfrac{\partial^2\psi}{\partial t^2}$, radians/sec^2
S	area, sq ft

t	time, sec
$t_{1/2}$	time to damp to one-half amplitude, sec
V	free-stream velocity, ft/sec
V_1, V_2	designations of vertical tails of two different areas
Y	lateral force, lb
α	angle of attack, deg
β	angle of sideslip, deg or radians
$\dot{\beta} = \frac{\partial \beta}{\partial t}$	
Λ	angle of sweepback, deg
ρ	mass density of air, slugs/cu ft
σ	angle of sidewash, deg
τ	time lag, $\frac{l_t}{V}$, sec
ψ	angle of yaw, deg
ω	circular frequency of oscillation, radians/sec

Subscripts:

F_1, F_2, F_3	denote fin used
t	tail
V_1, V_2	denote vertical tail used
w	wing

MODELS

Models With Auxiliary Fins

In this series of tests, a fuselage with each of two differently sized vertical tails was tested in combination with each of three auxiliary fins (fig. 2). This model, without the auxiliary fins, was used in the investigation of reference 3 where it is completely described. The fuselage was a round-nose body of revolution designated as F_4 in reference 3. The vertical tails, designated V_2 and V_3 in reference 3, are designated V_1 and V_2, respectively, in the course of this investigation. The tails were swept back 45° at the quarter-chord line and both had aspect ratios of 1. The vertical tail V_1 was 48.6 square inches in area whereas the vertical tail V_2 was 72.9 square inches in area. These tails had taper ratios of 0.6 and NACA 65A008 profiles in planes parallel to the fuselage center line. Although these tests were made without a wing or horizontal tail, an arbitrary wing area of 2.25 square feet and span of 3 feet were used for computational purposes. The fuselage and tails were constructed of laminated mahogany and, in combination, had an inertia in yaw I_Z of 0.34 slug-ft^2.

The auxiliary fins were mounted on the top of the fuselage with their quarter-chord lines at the assumed center of gravity of the model. These fins were rectangular in plan form, had a chord of 3 inches, and were cut from 1/8-inch-thick sheet aluminum. The fins, designated F_1, F_2, and F_3, were $1\frac{1}{2}$, 3, and 6 inches in span and had aspect ratios of 1/2, 1, and 2, respectively.

Models With Wings in Various Vertical Positions

The second method of varying the sidewash at the vertical tail was by the alteration of wing vertical position using two models for which the static effect of wing position on the sidewash was already available. This information is presented in reference 4 together with a complete description of the models. One of these models, hereafter called the straight-wing model, had unswept wing, vertical-tail, and horizontal-tail surfaces; the other model, hereafter called the swept-wing model, had wing and tail surfaces swept back 45° at the quarter-chord line (see figs. 3 and 4). Further geometric properties of the wings and vertical tails, both straight and swept, are given in the following table:

	Wings	Vertical tails
Aspect ratio	4.0	2.0
Taper ratio	0.6	0.6
Area, sq ft	2.25	0.337
Span, ft	3.0	0.822
Mean aerodynamic chord, ft	0.765	0.419
Airfoil section	NACA 65A008	NACA 65A008

The fuselage of these models was constructed in a manner such that the wing could be placed in any one of three vertical positions; these are called the low, middle, and high positions.

The models with the wings in various vertical positions were also constructed of laminated mahogany. The inertia in yaw for the complete models varied between $I_Z = 0.44$ and $I_Z = 0.50$ slug-ft^2 depending on the configuration and angle of attack.

APPARATUS

All tests were conducted in the 6- by 6-foot test section of the Langley stability tunnel. The steady-state stability characteristics of the models were determined from standard force tests wherein the model was mounted on a single-strut support at the assumed center of gravity and the forces and moments recorded for the test conditions by means of a conventional six-component balance. The steady-yawing derivatives of the models were obtained by the standard curved-flow testing procedure employed in the Langley stability tunnel.

The apparatus described in reference 5 was used to measure the oscillatory stability characteristics. The model was mounted on a strut which was free to rotate in yaw. The rotation was partly restrained and restoring moments were provided by means of flexure pivots which supported the oscillating strut. A mirror clamped to a section of the strut which extended outside the tunnel reflected a beam of light into an optical recorder. A continuous record of the motion of the model, after an initial displacement in yaw, was obtained on film. A timer in the recorder simultaneously exposed timing lines on the film in order that time, as well as model displacement, could be read. Variation of the period of oscillation for the wing-height models was accomplished by clamping weights to the oscillation strut outside the tunnel and thereby varying the yawing moment of inertia of the oscillating system. This procedure is fully described in reference 5.

TESTS

Force Tests

The model with auxiliary fins was tested without a wing and at an angle of attack of 0° through the range of static sideslip angles of $\pm 20^\circ$ for the fuselage alone, the fuselage with each of the vertical tails V_1 and V_2, and the fuselage and each of the vertical tails in combination with each of the auxiliary fins F_1, F_2, and F_3. The static sideslipping derivatives were derived from these data by measuring the variations of the rolling-moment, yawing-moment, and lateral-force coefficients through $\beta = \pm 5^\circ$. Because the sideslipping derivatives and the sidewash properties of the models with varying wing position were already available in reference 4, these models were not tested again.

The steady-yawing derivatives for all models were measured by means of the standard stability-tunnel curved-flow technique. Tunnel-wall curvatures were employed to correspond with values of the yawing-velocity parameter $\frac{rb}{2V}$ of 0, -0.0312, -0.0660, and -0.0868 for these models.

Oscillation Tests

The oscillation tests of the models with auxiliary fins were made in order to determine whether an effect of sidewash on the unsteady lateral damping of a model could be detected. These tests consisted of deflecting the model several degrees in yaw and then releasing it. The resulting oscillatory yawing motion of the model was allowed to damp to less than one-half its original amplitude. These tests were made, at about the same frequency of oscillation, for the fuselage and the larger vertical tail V_2 and the fuselage and V_2 in combination with each of the auxiliary fins F_1, F_2, and F_3. The period of oscillation for these tests was about 1.5 seconds which corresponds to a value of the reduced frequency of $k \approx 0.0045$.

The oscillation tests of the models with varying wing position were somewhat more elaborate tests and were similar to those of reference 5. These models were tested at four frequencies of oscillation covering the range of reduced frequencies from $k = 0.002$ to $k = 0.020$. The straight-wing model was tested for angles of attack of 0° and 8°, and the swept-wing model for angles of attack of 0° and 16°. The higher angles of attack are well below the stall for each model. (See ref. 4.) The wings of the models were tested in the low, middle, and high positions in order to vary the sidewash characteristics, and the approximate tail increments to the stability derivatives were obtained by testing the tail-on and the tail-off configurations.

Test Conditions

The tunnel conditions for all tests are tabulated below:

Type of test	Model with -	Dynamic pressure, lb/sq ft	Reynolds number	Wind velocity, ft/sec
Steady sideslipping	Auxiliary fins	25	710,000	145
	Varying wing position (data from ref. 4)	40	880,000	183
Steady yawing	Auxiliary fins	25	710,000	145
	Varying wing position	25	710,000	145
Oscillation	Auxiliary fins	4	284,000	58
	Varying wing position	25	710,000	145

Reduction of Oscillation Test Data

From the continuous film record taken of the motion of the model after an initial displacement, the amplitudes of the successive cycles were measured and plotted to a logarithmic scale against time. Inasmuch as the damping is logarithmic in nature, the resulting plot is a straight line from which may be read the time for the motion to damp to one-half amplitude $t_{1/2}$. The period and $t_{1/2}$ being known from the oscillation data, the unsteady damping in yaw and directional stability were calculated by using the expressions of reference 5.

$$C_{n_r} - C_{n_{\dot{\beta}}} = -\frac{2.772VI_Z}{qS_w b_w^2}\left[\frac{1}{t_{1/2}} - \left(\frac{1}{t_{1/2}}\right)_{\text{wind off}}\right]$$

$$C_{n_\beta} + C_{n_{\dot{r}}} k^2\left(\frac{b_w}{c_t}\right)^2 = \frac{1}{qS_w b_w}\left[I_Z(2\pi f)^2 + N_\psi\right]$$

The N_ψ term represents the mechanical spring constant of the flexure pivots and, for these tests, was 6.8 ft-lb/radian.

ANALYSIS

If unsteady-lift effects and induced-camber effects on the vertical tail are considered to be negligible, then the vertical-tail contribution to the yawing moment of an airplane is given, approximately, by the product of the lift-curve slope of the vertical tail, the effective angle of attack at the vertical tail, and the tail length:

$$C_n = - \frac{l_t}{b_w} C_{Y_\beta} \alpha_t \tag{1}$$

If a pure sideslipping motion is considered, the effective angle of attack of the vertical tail of an airplane performing such a motion is composed of a geometric angle β and an induced angle σ. This effective angle of attack during sideslipping may be written

$$\alpha_t(\beta) = \beta + \frac{\partial \sigma}{\partial \beta}\left(\beta - \frac{\partial \beta}{\partial t} \tau\right) \tag{2}$$

The sidewash at the vertical tail affects the yawing moment through a time lag τ because of the distance from the airplane center of gravity to the vertical tail. The effective angle of attack during sideslipping should therefore include this time lag in the manner of equation (2) where the term $\frac{\partial \sigma}{\partial \beta} \frac{\partial \beta}{\partial t} \tau$ is the lag of the sidewash term. This time lag may be approximated by $\tau = \frac{l_t}{V}$, whereupon equation (2) may now be written

$$\alpha_t(\beta) = \beta\left(1 + \frac{\partial \sigma}{\partial \beta}\right) + \dot{\beta}\left(- \frac{\partial \sigma}{\partial \beta} \frac{l_t}{V}\right) \tag{3}$$

The partial derivative of equation (1) with respect to β then leads to the directional-stability parameter

$$C_{n_\beta} = - \frac{l_t}{b_w} C_{Y_\beta}\left(1 + \frac{\partial \sigma}{\partial \beta}\right) \tag{4}$$

The derivative of equation (1) with respect to $\frac{\dot{\beta} b}{2V}$ leads to the damping in yaw during oscillatory sideslipping

$$C_{n_{\dot{\beta}}} = 2\left(\frac{l_t}{b_w}\right)^2 C_{Y_\beta} \frac{\partial \sigma}{\partial \beta} \tag{5}$$

If a pure yawing motion is considered, the effective angle of attack of the vertical tail of the airplane for this motion including the lag term is

$$\alpha_t(\psi) = -\frac{\dot{\psi} l_t}{V} + \frac{\partial \sigma}{\partial \dot{\psi}}\left(\dot{\psi} - \frac{\partial \dot{\psi}}{\partial t}\tau\right) \tag{6}$$

Since $\dot{\psi} = r$, then

$$\alpha_t(\psi) = r\left(-\frac{l_t}{V} + \frac{\partial \sigma}{\partial r}\right) - \frac{\partial \sigma}{\partial r}\frac{\partial r}{\partial t}\frac{l_t}{V} \tag{7}$$

The examination of a large quantity of data obtained in steady yawing flow in the Langley stability tunnel indicates no important influence of the $\frac{\partial \sigma}{\partial r}$ term for usual airplane configurations. This quantity will therefore be assumed to be insignificant in magnitude and will be neglected. Equation (7) therefore becomes simply

$$\alpha_t(\psi) = -2\frac{l_t}{b_w}\frac{r b_w}{2V} \tag{8}$$

which is also true for steady yawing motion. The rate of change of the yawing-moment coefficient of equation (1) with the yawing-velocity parameter results in the damping in yaw during the pure yawing motion

$$C_{n_r} = 2\left(\frac{l_t}{b_w}\right)^2 C_{Y_\beta} \tag{9}$$

For the oscillatory motion given the models in these tests, wherein $\psi = -\beta$, the total damping in yaw of the vertical tail of the oscillating model is given by the algebraic sum of the derivatives C_{n_r} and $C_{n_{\dot{\beta}}}$. Therefore,

$$C_{n_r} - C_{n_{\dot{\beta}}} = 2\left(\frac{l_t}{b_w}\right)^2 C_{Y_\beta}\left(1 - \frac{\partial \sigma}{\partial \beta}\right) \tag{10}$$

For the case of steady sideslipping or yawing motions, the important difference in the above development lies in the fact that the lag of the sidewash term in equation (2) is zero. The result then is that

$$C_{n_{\dot{\beta}}} = 0$$

and the steady-state damping in yaw is given by equation (9). It will be noted that equation (4) for the directional stability remains the same for the steady motion as that for the oscillatory motion.

The significance of this preliminary discussion is that, for unsteady motion, the lateral damping is expected to be increased over the steady damping by the factor $1 - \frac{\partial \sigma}{\partial \beta}$ because of the lag of the sidewash. This result was, of course, shown in reference 1 in connection with the effect of the lag of the downwash on the damping in pitch of a horizontal tail. The directional stability of a vertical tail is expected to vary as the factor $1 + \frac{\partial \sigma}{\partial \beta}$ in both steady and unsteady motion. This effect is, however, only due to the static sidewash angle and is not associated with the lag of the sidewash.

The results of reference 5 show that the total damping in yaw for an oscillating model, wherein $\psi = -\beta$, is given by

$$C_{n_r} - C_{n_{\dot{\beta}}}$$

and the total directional stability for the same motion by

$$C_{n_\beta} + k^2\left(\frac{b_w}{c_t}\right)^2 C_{n_{\dot{r}}}$$

The $C_{n_{\dot{\beta}}}$ and $C_{n_{\dot{r}}}$ terms arise because of the translational and rotary accelerations of the model and they become zero in steady flow. For frequencies of oscillation corresponding to those used in this investigation and for the wingless model at zero angle of attack, reference 5 indicates that the $C_{n_{\dot{\beta}}}$ term is small when compared with the C_{n_r} portion of the damping in yaw. However, certain tests (ref. 6, for example) have also indicated that the $C_{n_{\dot{\beta}}}$ derivative, which is the oscillatory portion of the damping in yaw, can become very large for a sweptback wing at high angles of attack.

References 5 and 7 show that the $C_{n_{\dot{r}}}$ portion of the directional stability is very small for the range of frequencies and the tail lengths being considered. For this reason $C_{n_{\dot{r}}}$ will be neglected in this paper and C_{n_β} will be used to represent both the static and the oscillatory directional stability.

RESULTS AND DISCUSSION

Model With Auxiliary Fins

The force and moment data from which the values of $\frac{\partial\sigma}{\partial\beta}$ were deduced for the various fin-tail combinations are shown in figures 5 to 8. These figures represent the variations of lateral-force, rolling-moment, and yawing-moment coefficients with static angles of sideslip between $\pm 20^\circ$ for the fuselage alone and the fuselage with each of the vertical tails (fig. 5), the fuselage with each of the auxiliary fins (fig. 6), the fuselage and auxiliary fins in combination with the small vertical tail (fig. 7), and the fuselage and auxiliary fins in combination with the large vertical tail (fig. 8). In these figures, the small vertical tail is designated V_1, the large vertical tail V_2, and the auxiliary fins F_1, F_2, and F_3, F_1 being the smallest fin and F_3 the largest.

From these data, the vertical-tail contribution to the yawing-moment coefficient was determined and is shown in figure 9 for both the auxiliary-fins-off and the auxiliary-fins-on configurations. The yawing-moment increment due to the interference of the auxiliary fins corresponds to an additional angle of attack at the vertical tail which is termed the sidewash angle and is represented in figure 9 by σ. The measured values of the slopes $\frac{\partial\sigma}{\partial\beta}$, which are generally constant between sideslip angles of $\pm 4^\circ$, are also shown in figure 9 for the various auxiliary-fin–vertical-tail combinations. The slopes $\frac{\partial\sigma}{\partial\beta}$ are shown (fig. 10) to vary almost linearly with the aspect ratios of the auxiliary fins.

The values of the yawing derivatives calculated by the simple expressions of reference 8 (by using a calculated value of C_{Y_β}) are shown in figure 11 for both the steady and oscillatory cases. The oscillatory values are obtained by multiplying the steady values by the appropriate experimental factors $1 - \frac{\partial\sigma}{\partial\beta}$ to include the lag of the sidewash effect. Shown also in figure 11 are the results of the verification experiments conducted. The steady-state data, obtained by the curved-flow testing procedure, indicate no effect of sidewash on the yawing derivatives. This result is reasonable since the fins, being at the assumed center of gravity of the model, have effectively zero angle of attack; hence no large disturbance exists such as that due to the angle of sideslip in the oscillation tests. The oscillation data, obtained by the free-oscillation technique, indicate an effect of the lag of the sidewash on the damping in yaw which is caused by the sideslip angle. This effect is consistent

with the variation calculated by including the sidewash factor measured by static sideslip tests. The freely damped oscillation tests were made only for the model with the large vertical tail.

Figure 12 is a similar figure for the sideslipping derivatives for which lag of sidewash does not enter the picture. The effect of sidewash is that due to the static sidewash which exists under both steady and oscillatory conditions. The calculated derivatives are, therefore, affected in both cases by the factor $1 + \frac{\partial \sigma}{\partial \beta}$. The experimental derivatives, both static and oscillatory, substantiate these trends. It will be noted, in figure 12, that the sidewash had an adverse effect on the directional stability of the models. At values of A_F close to unity, the sidewash was strong enough to destroy the stability of the model and, at higher values of A_F, to render the model directionally unstable.

Some differences in magnitude beyond those due to sidewash lag may be noted between the oscillatory and the steady experimental values of the damping in yaw and the directional stability. These differences may be due to the very low Reynolds number of the oscillation data.

Model With Wings in Various Vertical Positions

The information regarding the static stability characteristics of the models with varying wing position and the effects of sidewash on these characteristics is presented in reference 4. Figure 13, from the data of reference 4, illustrates the sidewash at the tail for both the straight-wing and the swept-wing models through an angle-of-attack range. The largest negative values of $\frac{\partial \sigma}{\partial \beta}$ are those which occur for the high-wing position. These values become very large at high angles of attack and are of the same order of magnitude as the values realized from the auxiliary fins.

The oscillatory damping in yaw and directional stability are presented, respectively, in figures 14 and 15 for both the straight-wing and swept-wing models. These tests were made for four frequencies of oscillation in both the tail-off and tail-on configurations. Each model was tested at two angles of attack; these angles were 0° and 8° for the straight-wing model and 0° and 16° for the swept-wing model. Shown also in figures 14 and 15 are the steady-state lateral derivatives for comparison with the oscillatory derivatives. These values are indicated as $k = 0$ values. The steady-state yawing derivatives were measured by the curved-flow testing procedure; the static sideslipping derivatives were obtained in reference 4.

The oscillatory yawing data is somewhat erratic but, in general, again indicates the increase in lateral damping consistent with the variation of $1 - \frac{\partial\sigma}{\partial\beta}$. This effect is particularly evident for the swept wing at $\alpha = 16^\circ$ where the sidewash gradient is especially strong. The large difference in magnitude between the steady damping C_{n_r} and the oscillatory damping $C_{n_r} - C_{n_{\dot{\beta}}}$ which is shown by both the tail-off and tail-on data for the swept-wing model at $\alpha = 16^\circ$ is thought to be a contribution of the wing itself. Some evidence of such a wing contribution to the oscillatory damping in yaw of a swept wing at high angles of attack is shown in the results of reference 6. It is possible that the vortex flow over a sweptback wing is influenced by the oscillatory motion in such a manner as to introduce a lag effect of its own and thereby contribute to the $C_{n_{\dot{\beta}}}$ damping derivative for the wing.

The oscillatory values of the directional stability have about the same variation with wing height as the steady-state ($k = 0$) data; these oscillatory values are, however, somewhat larger in magnitude than the steady-state values and indicate a somewhat greater directional stability under oscillatory conditions.

The contributions of the vertical tails to the damping in yaw and the directional stability were obtained by subtracting the tail-off data of figures 14 and 15 from the complete-model data. These results are shown for the damping in yaw in figure 16. The experimental values shown in figure 16(a) again indicate, in general, the variation of the oscillatory damping in the manner of $1 - \frac{\partial\sigma}{\partial\beta}$, whereas the steady-state data show no such variation because of the absence of sidewash due to β. This effect is particularly evident at $\alpha = 16^\circ$ for the swept wing and must be attributed to an increase in the magnitude of the damping derivative $C_{n_{\dot{\beta}_t}}$ which exists during this type of oscillation testing. During steady-yawing tests, β and $C_{n_{\dot{\beta}}}$ are, of course, zero. In figure 16(b) are shown the values of the vertical-tail damping calculated by the method described in references 5 and 7 which uses the unsteady circulation functions of reference 9. These calculated values were multiplied by the appropriate experimental factors $1 - \frac{\partial\sigma}{\partial\beta}$. In general, the trends of the oscillation data with varying wing position are consistent with those calculated. No consistent effect of frequency on the oscillatory damping in yaw was evident in the range of frequency covered by these experiments.

Figure 17 is a similar figure for the directional stability. Figure 17(a) represents the experimental results, both static and oscillatory. The calculated results, using the unsteady-lift theory values multiplied

by the appropriate $1 + \frac{\partial\sigma}{\partial\beta}$ factors, are shown in figure 17(b). Both the static and the oscillatory tail contributions to the directional stability exhibit qualitatively the same variations with the sidewash parameter as were predicted by using the factor $1 + \frac{\partial\sigma}{\partial\beta}$.

In figure 18, the steady and the oscillatory damping in yaw of the swept-wing model is shown directly as a function of wing position for a representative value of the reduced frequency, $k = 0.018$. For $\alpha = 16^\circ$, two differences between the steady damping C_{n_r} and the oscillatory damping $C_{n_r} - C_{n_{\dot\beta}}$ are most evident. There appears, first of all, the difference between the steady and oscillatory data for both the tail-off and the tail-on damping which is the oscillatory wing contribution discussed previously in this paper. The second difference is the lag of the sidewash effect which appears during oscillation because of the presence of sidewash due to β. The same trend took place to a smaller extent for $\alpha = 0^\circ$. The curves, shown as calculated in figure 18, were obtained by measuring the difference between the tail-on and tail-off curved-flow damping, multiplying this difference by appropriate values of $1 - \frac{\partial\sigma}{\partial\beta}$, and adding these tail contributions to the oscillatory tail-off values. The trends appear to be about the same as those for the experimental tail-on oscillation data.

Figure 19 is a similar figure for the directional stability. The decrease in directional stability which takes place when the wing is moved from the low to the high position is about the same during steady and oscillation testing. The calculated curves, for this figure, were established by estimating a value of C_{Y_β} from reference 10, and multiplying the value obtained by the appropriate tail-length factors and measured values of $1 + \frac{\partial\sigma}{\partial\beta}$. These calculated tail contributions were then added to the experimental wing-fuselage contributions.

CONCLUSIONS

The results of tests in which the damping in yaw and the directional stability of airplane models with vertical tails in the presence of sidewash were measured in both steady and oscillatory flow indicate the following conclusions:

1. The vertical-tail contribution to the oscillatory lateral damping is dependent upon the factor $1 - \frac{\partial \sigma}{\partial \beta}$ as analytically predicted $\left(\frac{\partial \sigma}{\partial \beta}\right.$ is the rate of change of the angle of sidewash with angle of sideslip$\left.\right)$. This factor represents the influence of the lag of the sidewash. The steady-state lateral damping is independent of the lag of the sidewash.

2. The vertical-tail contribution to the directional stability is dependent upon the factor $1 + \frac{\partial \sigma}{\partial \beta}$ under both steady and oscillatory conditions because of the effect of the static sidewash.

3. No consistent effect of frequency on the oscillatory damping in yaw was evident in the range of frequency of this investigation.

4. The 45° sweptback-wing model at an angle of attack of 16° exhibited values of the oscillatory damping in yaw which were much larger than corresponding values of the steady-state damping in yaw. This increase in damping is believed to be the contribution of the wing itself to the yawing moment due to sideslipping acceleration.

Langley Aeronautical Laboratory,
National Advisory Committee for Aeronautics,
Langley Field, Va., October 1, 1954.

REFERENCES

1. Cowley, W. L., and Glauert, H.: The Effect of the Lag of the Downwash on the Longitudinal Stability of an Aeroplane and on the Rotary Derivative M_q. R. & M. No. 718, British A.R.C., 1921.

2. Jones, Robert T., and Fehlner, Leo F.: Transient Effects of the Wing Wake on the Horizontal Tail. NACA TN 771, 1940.

3. Queijo, M. J., and Wolhart, Walter D.: Experimental Investigation of the Effect of Vertical-Tail Size and Length and of Fuselage Shape and Length on the Static Lateral Stability Characteristics of a Model With 45° Sweptback Wing and Tail Surfaces. NACA Rep. 1049, 1951. (Supersedes NACA TN 2168.)

4. Goodman, Alex: Effects of Wing Position and Horizontal-Tail Position on the Static Stability Characteristics of Models With Unswept and 45° Sweptback Surfaces With Some Reference to Mutual Interference. NACA TN 2504, 1951.

5. Bird, John D., Fisher, Lewis R., and Hubbard, Sadie M.: Some Effects of Frequency on the Contribution of a Vertical Tail to the Free Aerodynamic Damping of a Model Oscillating in Yaw. NACA Rep. 1130, 1953. (Supersedes NACA TN 2657.)

6. Bird, John D., Jaquet, Byron M., and Cowan, John W.: Effect of Fuselage and Tail Surfaces on Low-Speed Yawing Characteristics of a Swept-Wing Model As Determined in Curved-Flow Test Section of the Langley Stability Tunnel. NACA TN 2483, 1951. (Supersedes NACA RM L8G13.)

7. Fisher, Lewis R.: Some Effects of Aspect Ratio and Tail Length on the Contribution of a Vertical Tail to Unsteady Lateral Damping and Directional Stability of a Model Oscillating Continuously in Yaw. NACA TN 3121, 1954.

8. Bamber, Millard J.: Effect of Some Present-Day Airplane Design Trends on Requirements for Lateral Stability. NACA TN 814, 1941.

9. Biot, M. A., and Boehnlein, C. T.: Aerodynamic Theory of the Oscillating Wing of Finite Span. GALCIT Rep. No. 5, Sept. 1942.

10. Queijo, M. J., and Riley, Donald R.: Calculated Subsonic Span Loads and Resulting Stability Derivatives of Unswept and 45° Sweptback Tail Surfaces in Sideslip and in Steady Roll. NACA TN 3245, 1954.

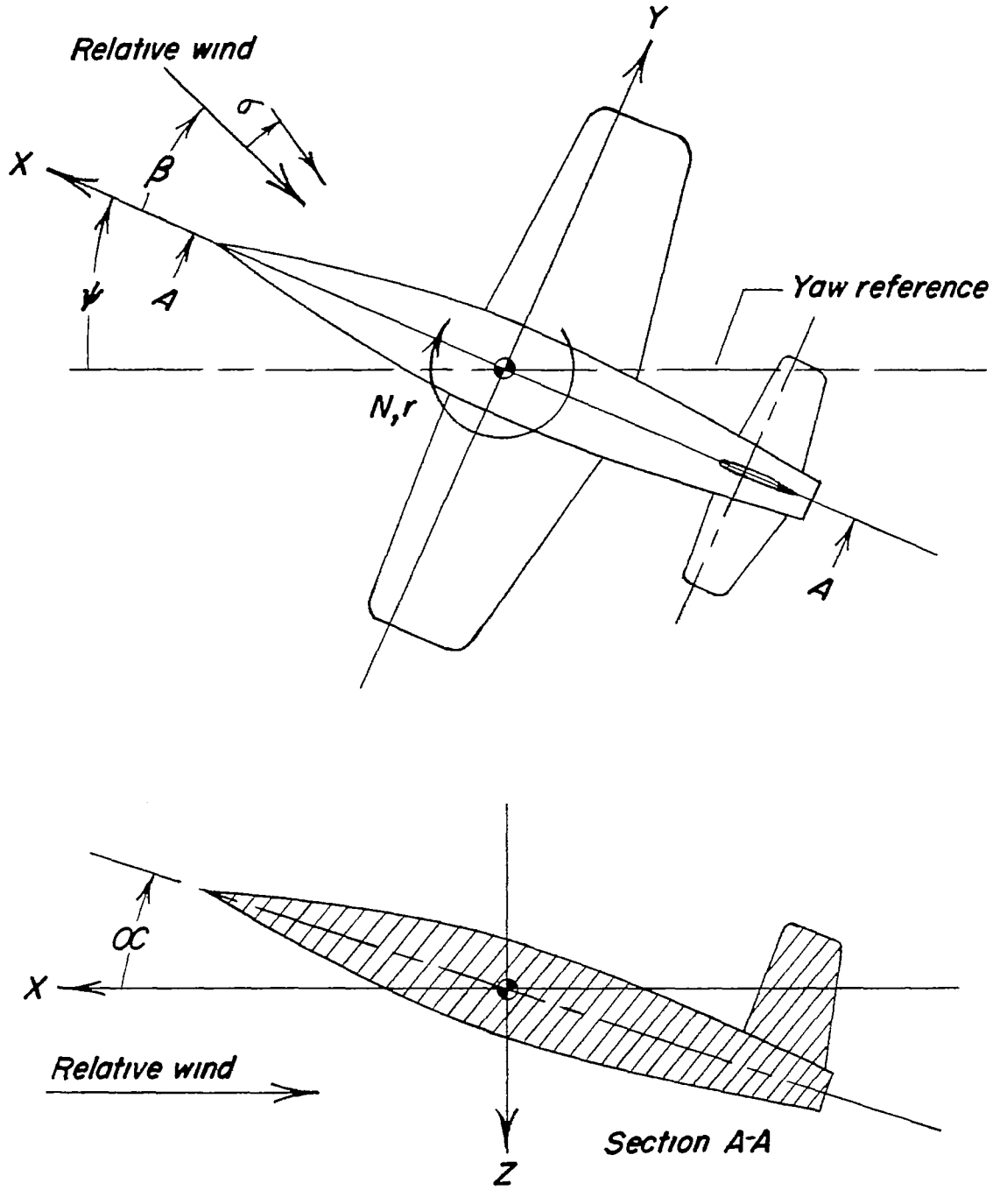

Figure 1.- System of stability axes. Arrows indicate positive forces, moments, and angular displacements. Yaw reference is generally chosen to coincide with initial relative wind.

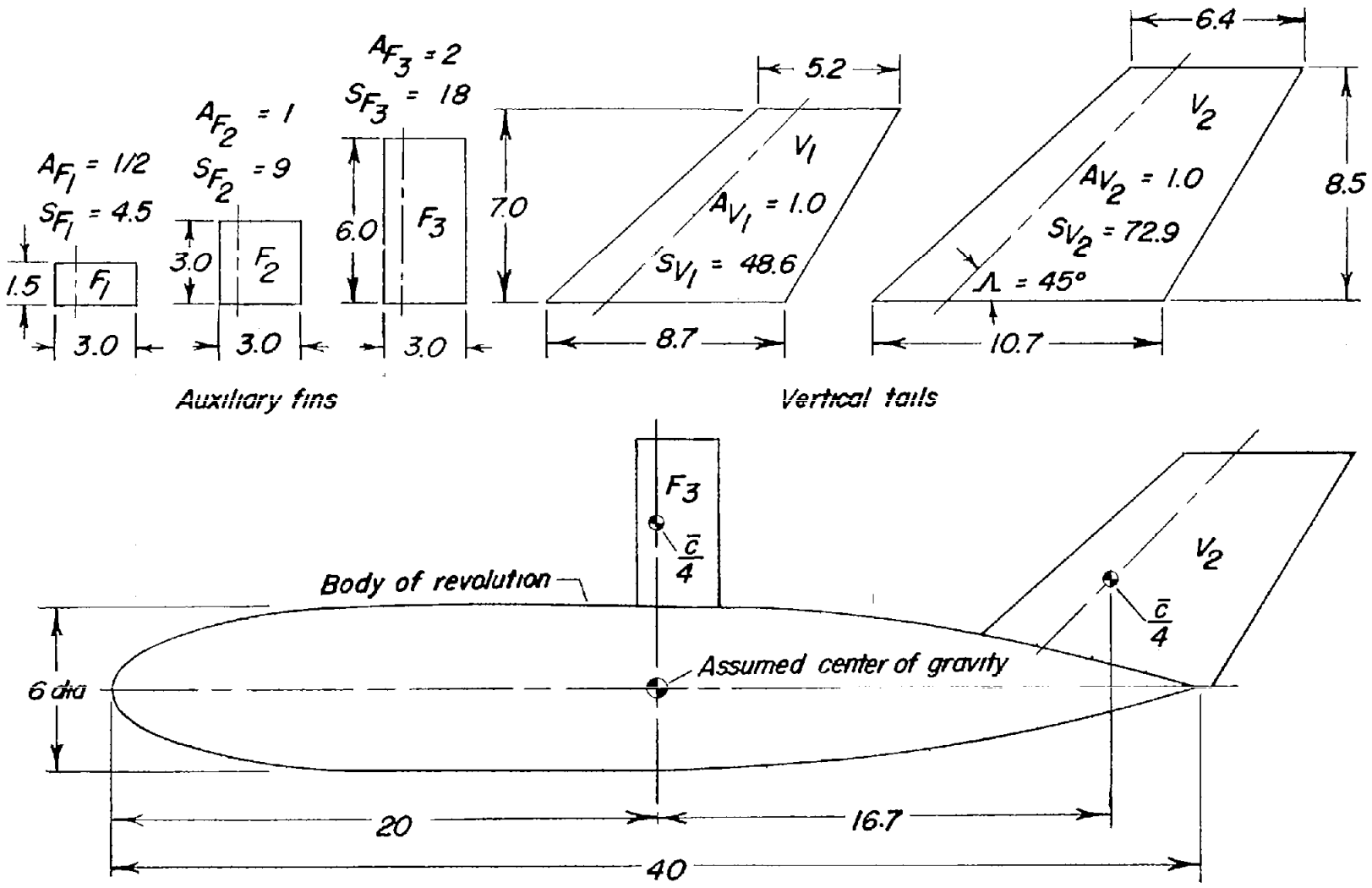

Figure 2.- Drawing of model showing auxiliary fins. All dimensions are in inches unless otherwise noted.

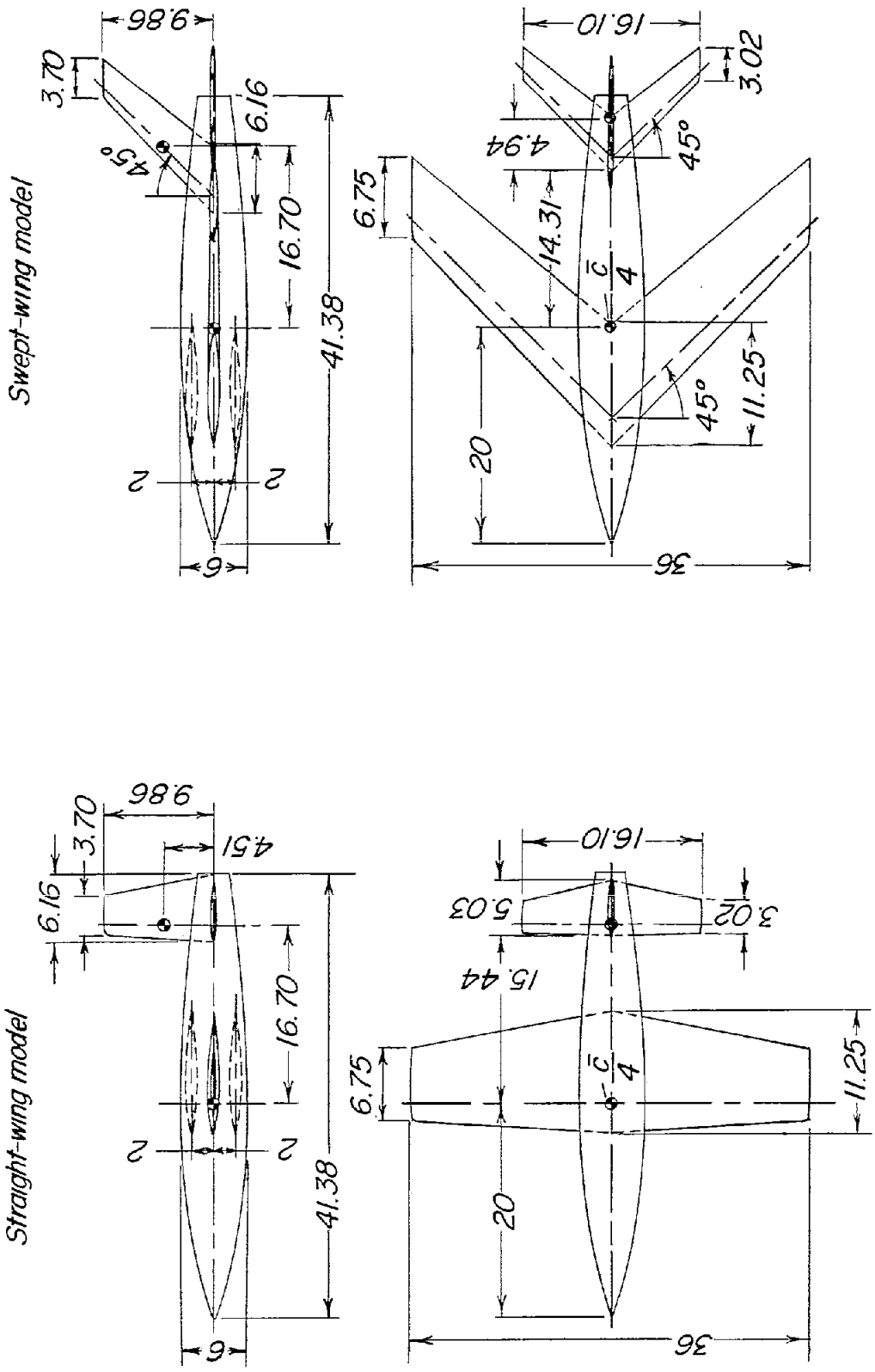

Figure 3.- Drawing of models with wing in various vertical positions. All dimensions are in inches unless otherwise noted.

L-70916

(a) Straight-wing model with wing in low position.

Figure 4.- Photographs of models with varying wing position mounted on free-oscillation strut in Langley stability tunnel.

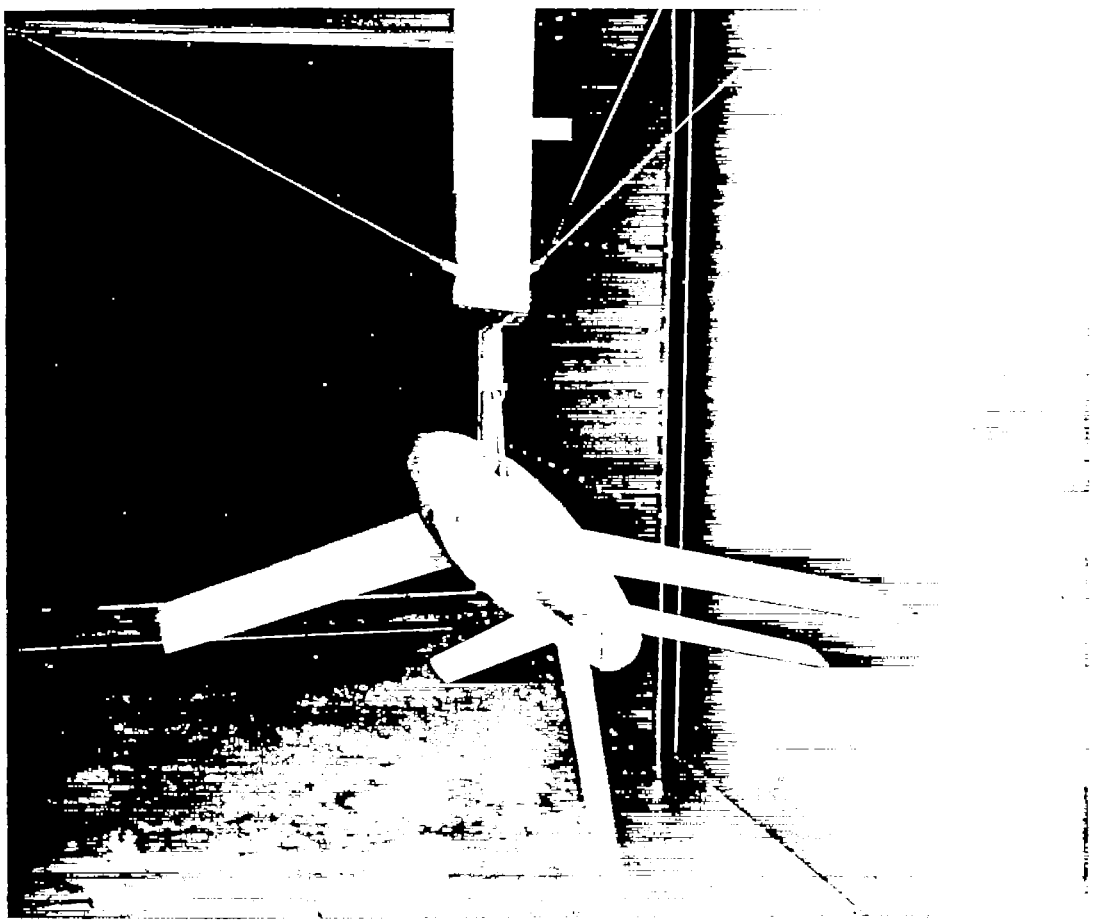

L-70917

(b) Swept-wing model with wing in high position.

Figure 4.- Concluded.

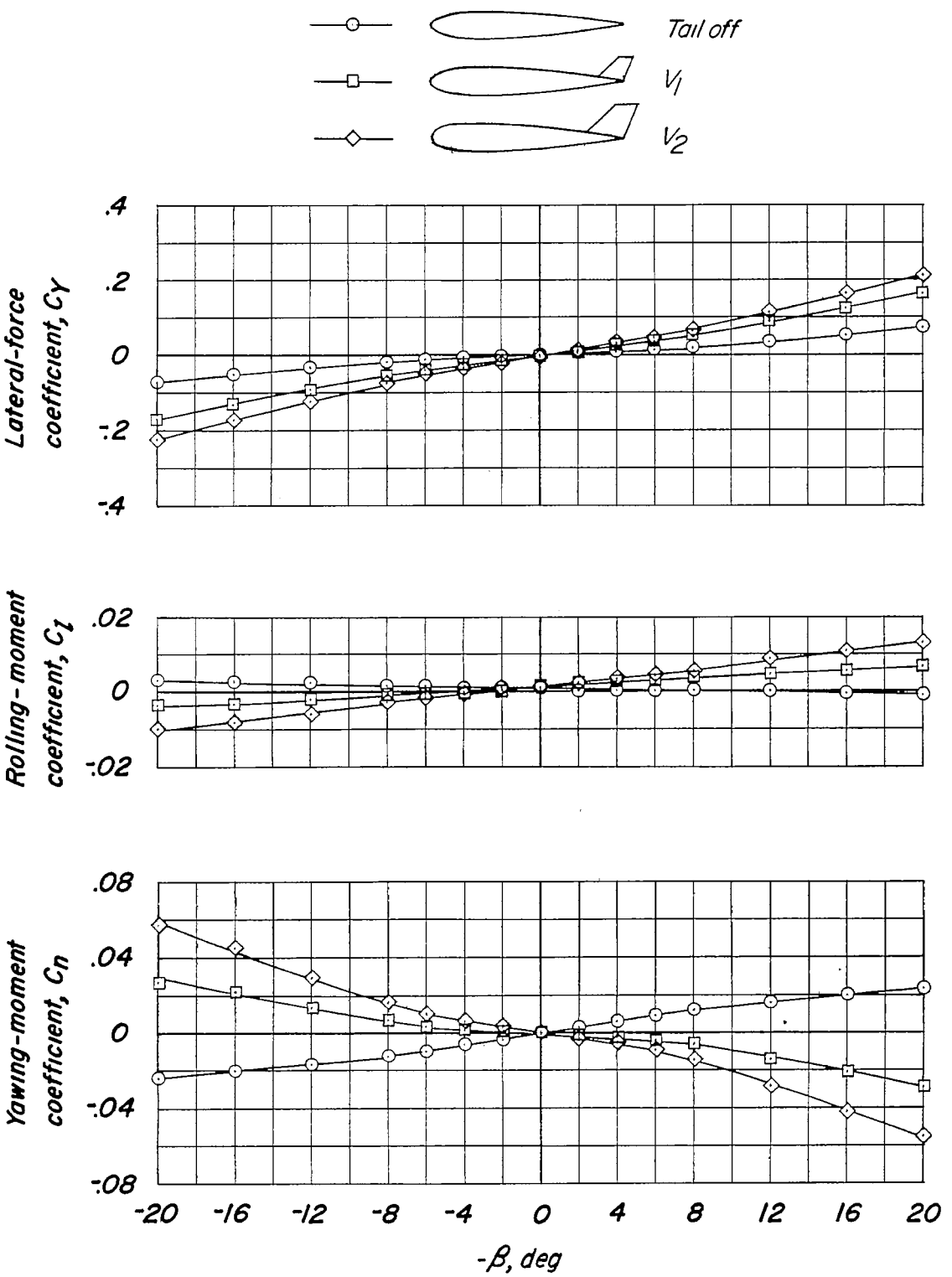

Figure 5.- Static sideslipping data for model with auxiliary fins. Fuselage alone and fuselage with each of the vertical tails.

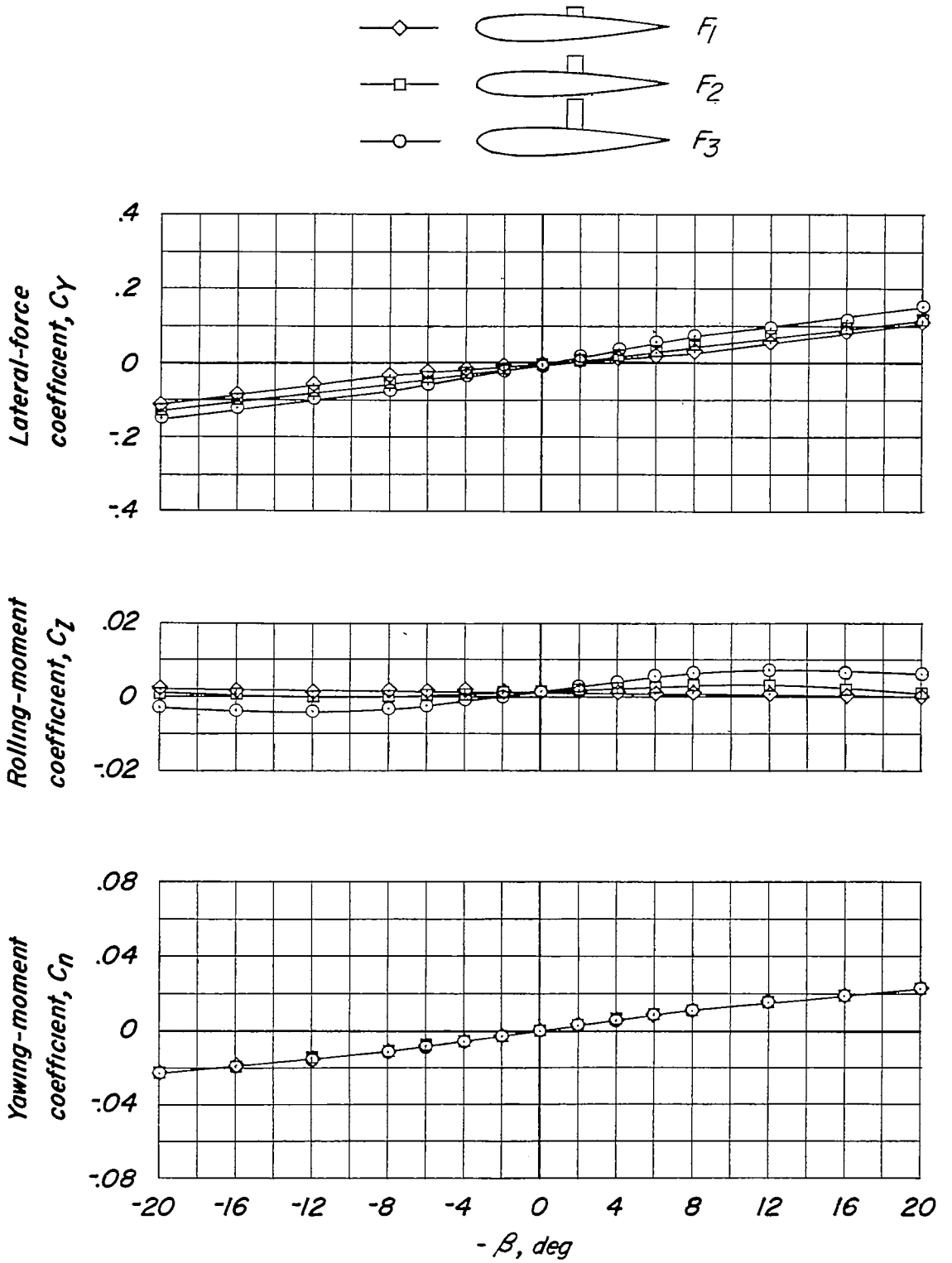

Figure 6.- Static sideslipping data for model with auxiliary fins. Fuselage with each of the auxiliary fins; tail off.

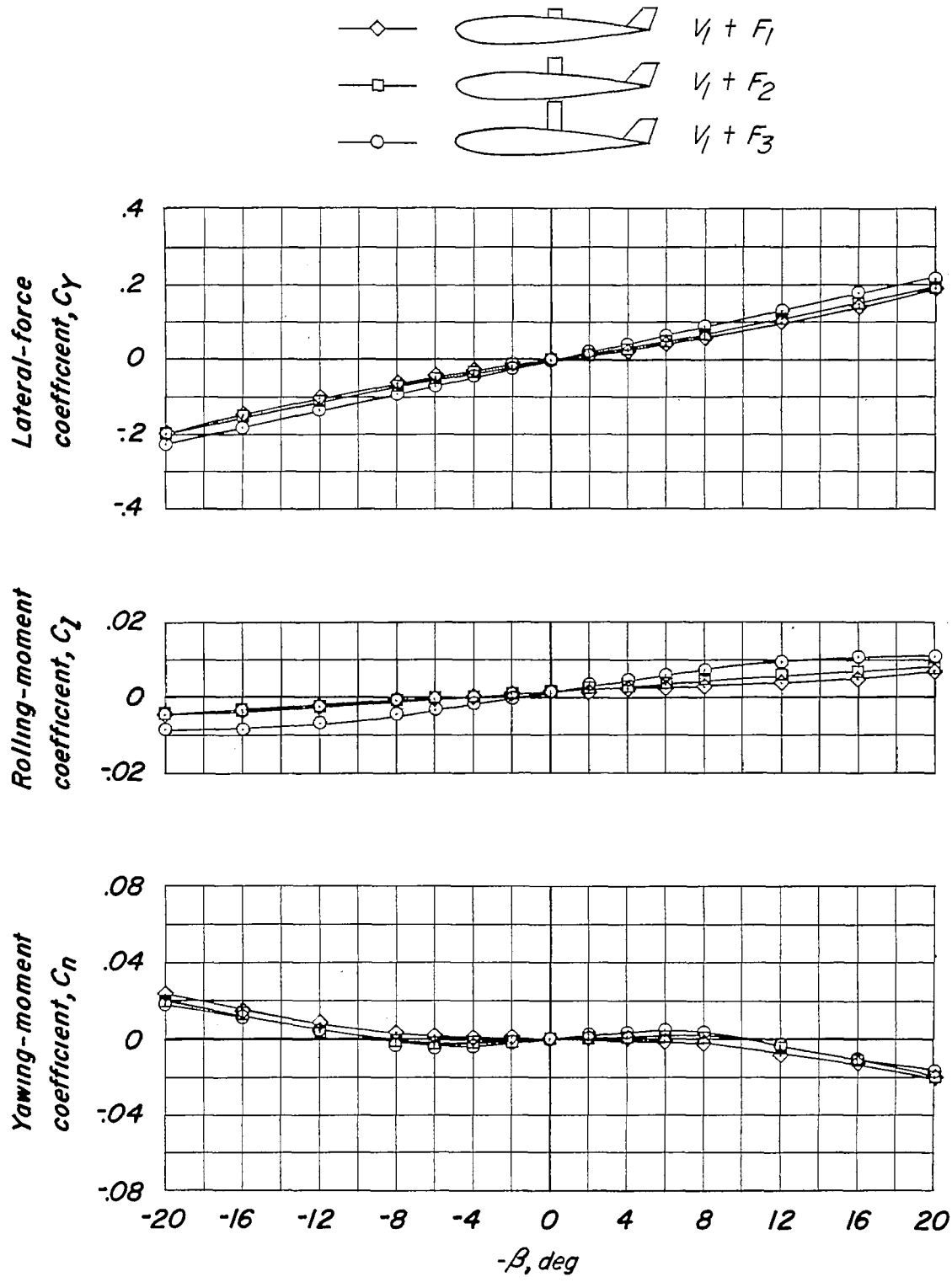

Figure 7.- Static sideslipping data for model with auxiliary fins. Fuselage with each auxiliary fin in combination with small vertical tail.

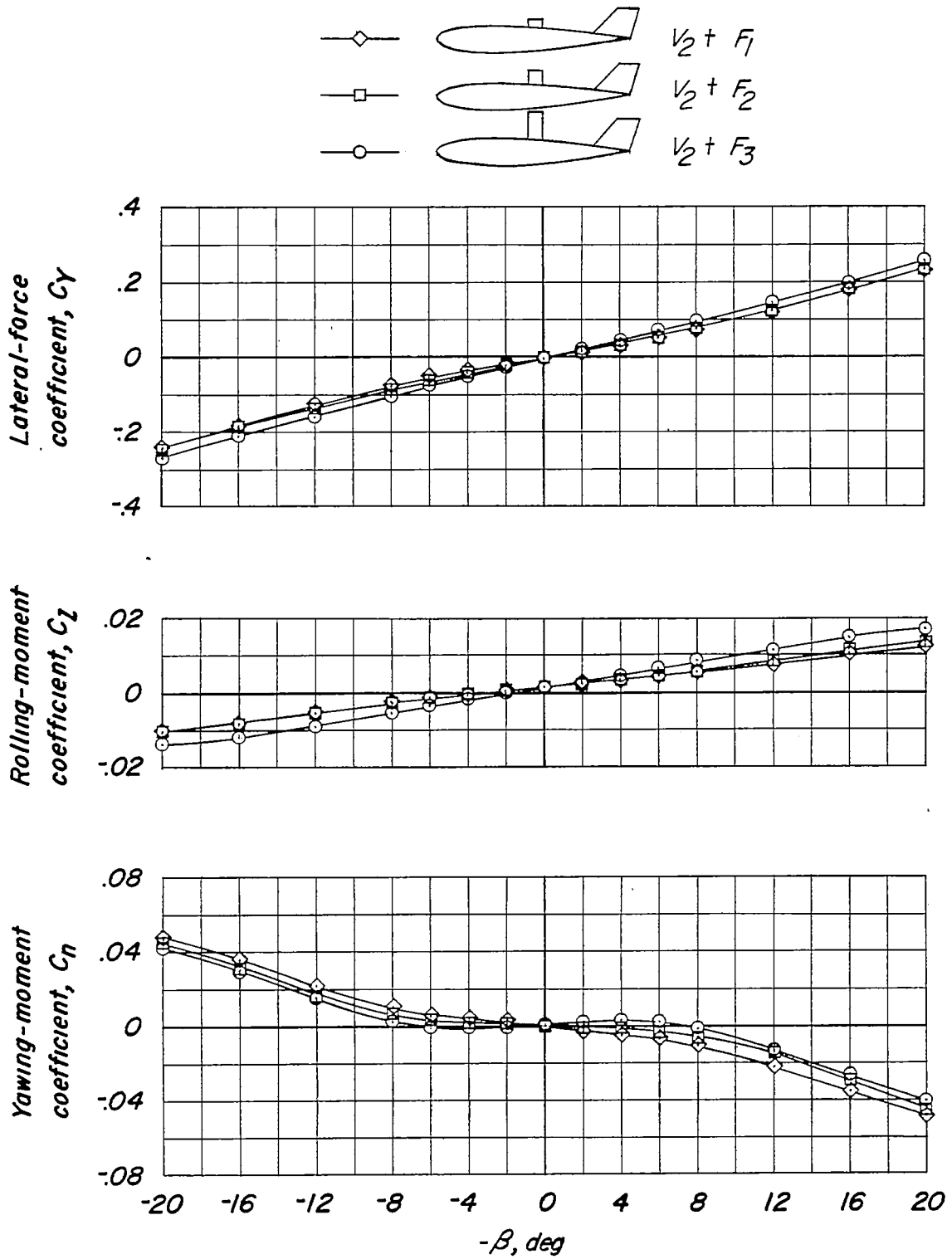

Figure 8.- Static sideslipping data for model with auxiliary fins. Fuselage with each auxiliary fin in combination with large vertical tail.

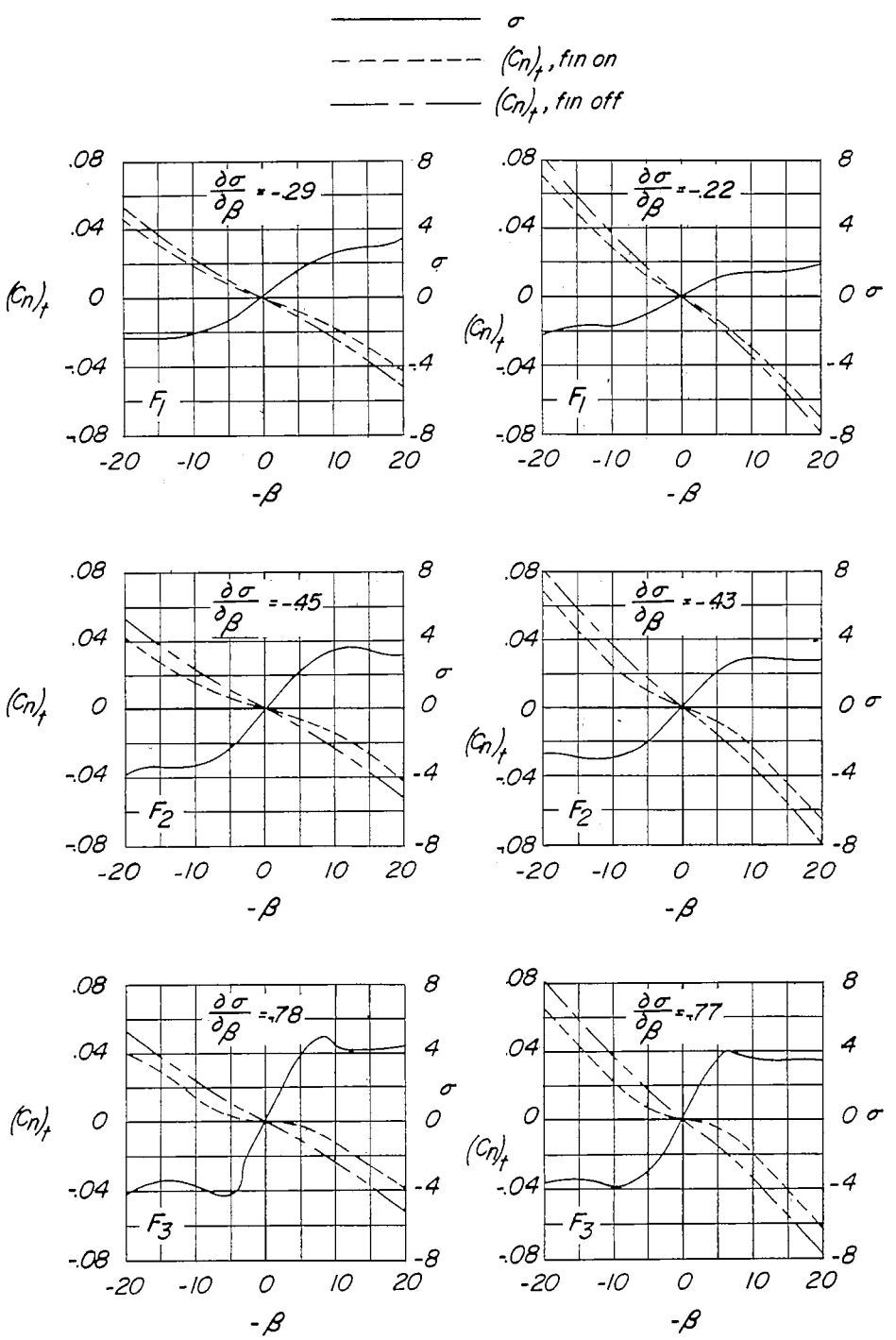

(a) Small vertical tail, V_1. (b) Large vertical tail, V_2.

Figure 9.- The effect of sideslip angle on the vertical-tail increments to the yawing-moment coefficient resulting from the auxiliary fins and on the sidewash due to the auxiliary fins.

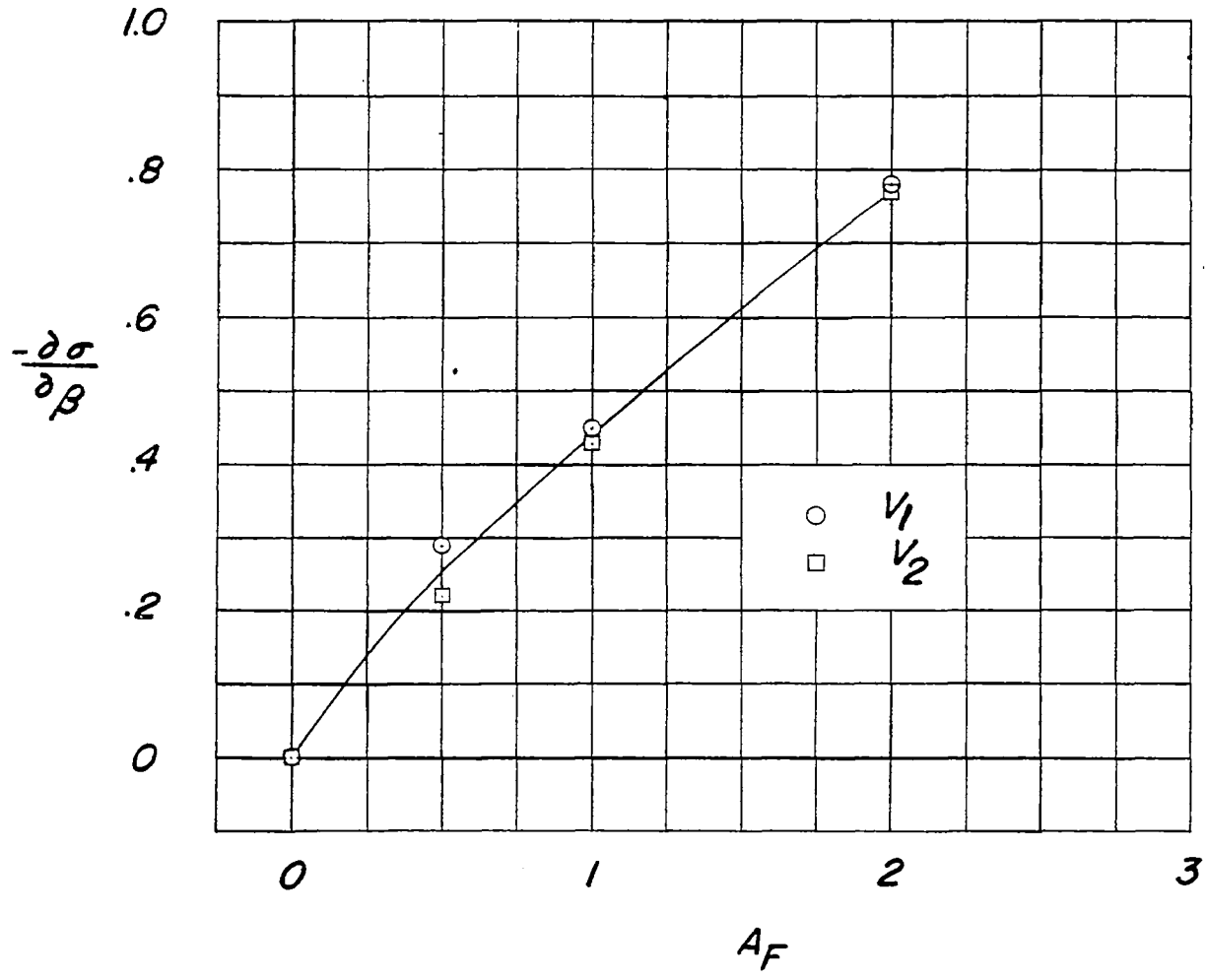

Figure 10.- The effect of aspect ratio of auxiliary fin on the rate of change of sidewash with angle of sideslip.

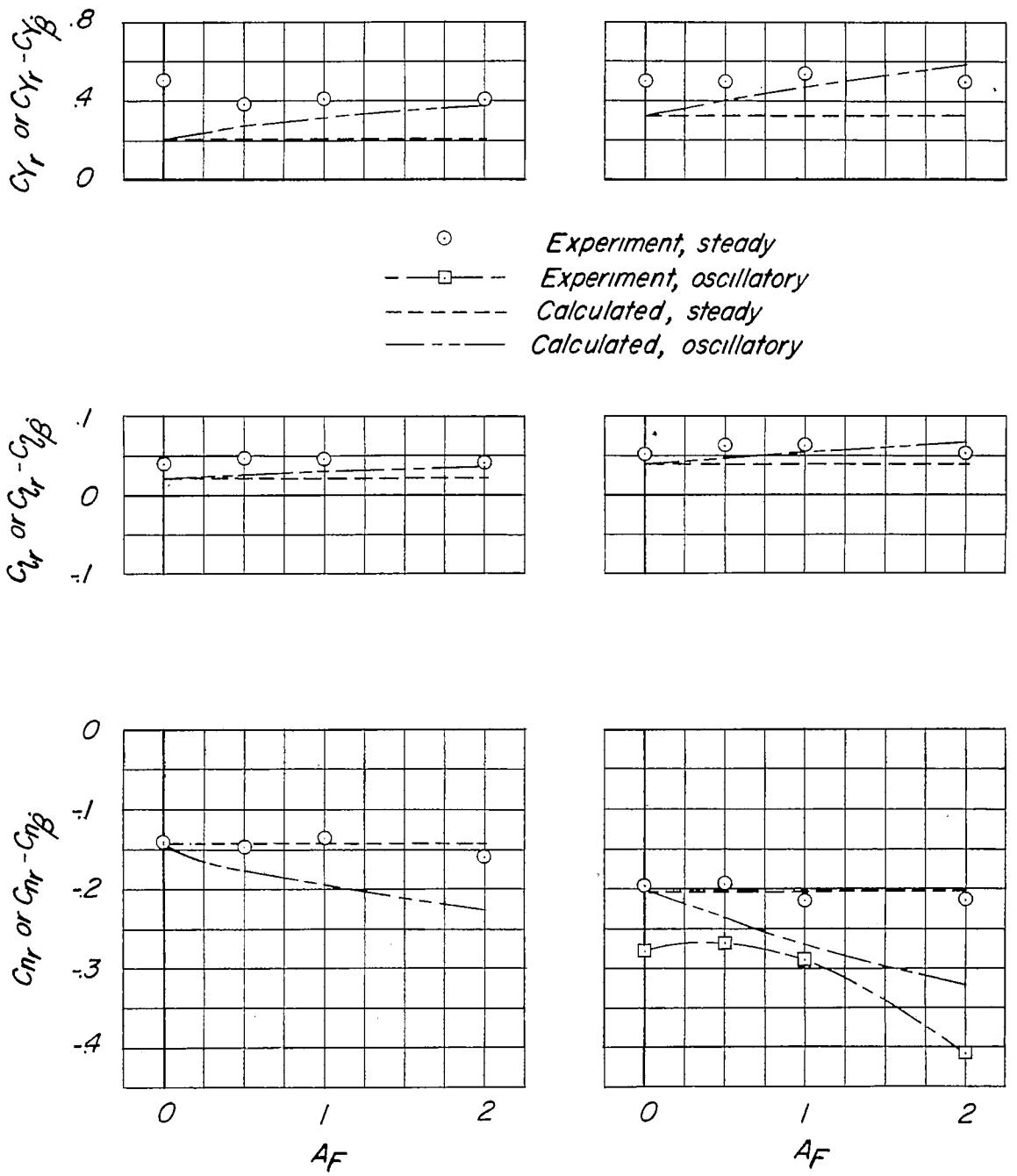

(a) Small vertical tail, V_1. (b) Large vertical tail, V_2.

Figure 11.- The experimental and calculated effects of the lag of the sidewash on the yawing derivatives of the model with auxiliary fins under both steady and oscillatory conditions. $k \approx 0.0045$.

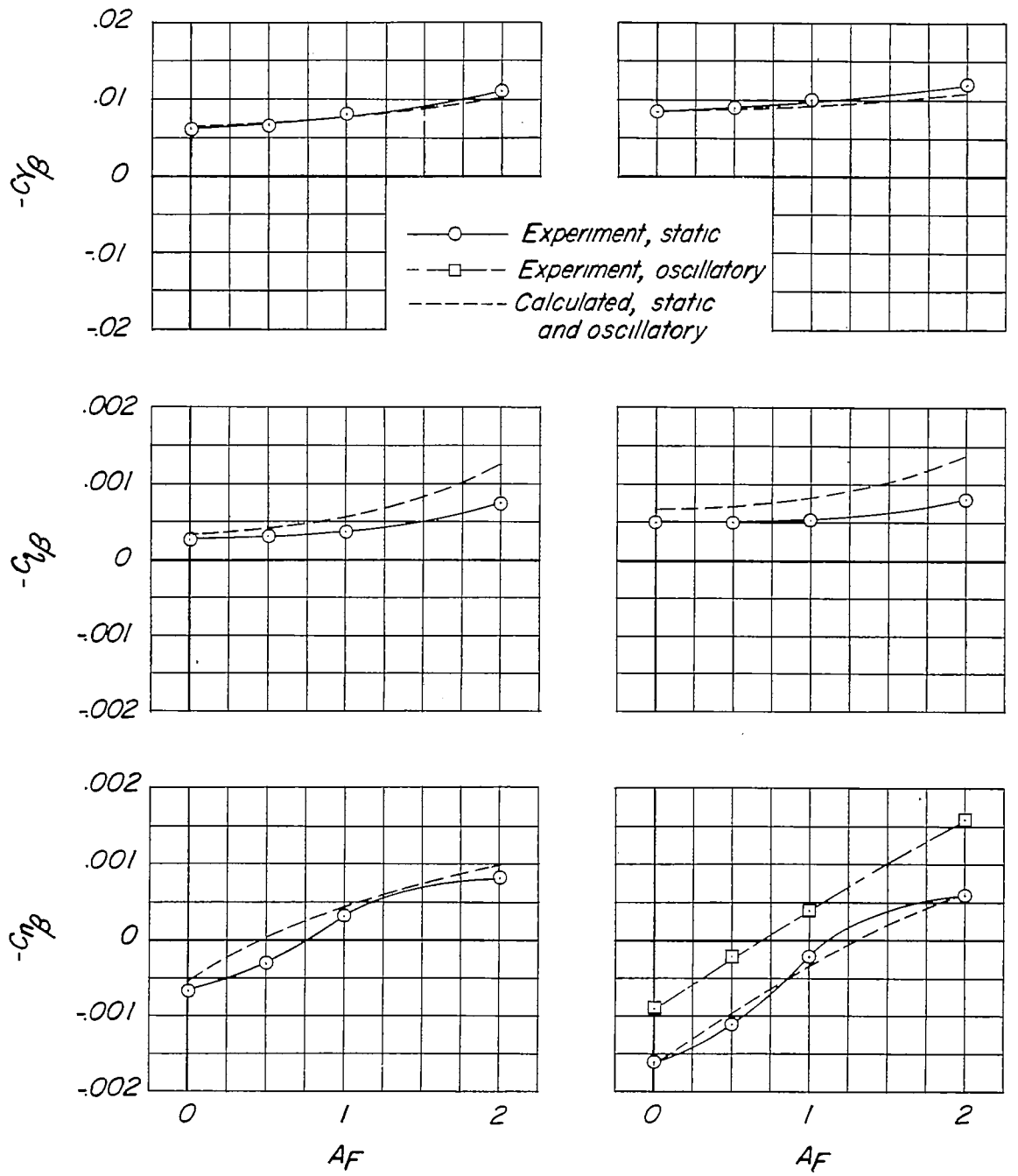

(a) Small vertical tail, V_1. (b) Large vertical tail, V_2.

Figure 12.- The experimental and calculated effects of the sidewash on the sideslipping derivatives of the model with auxiliary fins under both steady and oscillatory conditions. $k \approx 0.0045$.

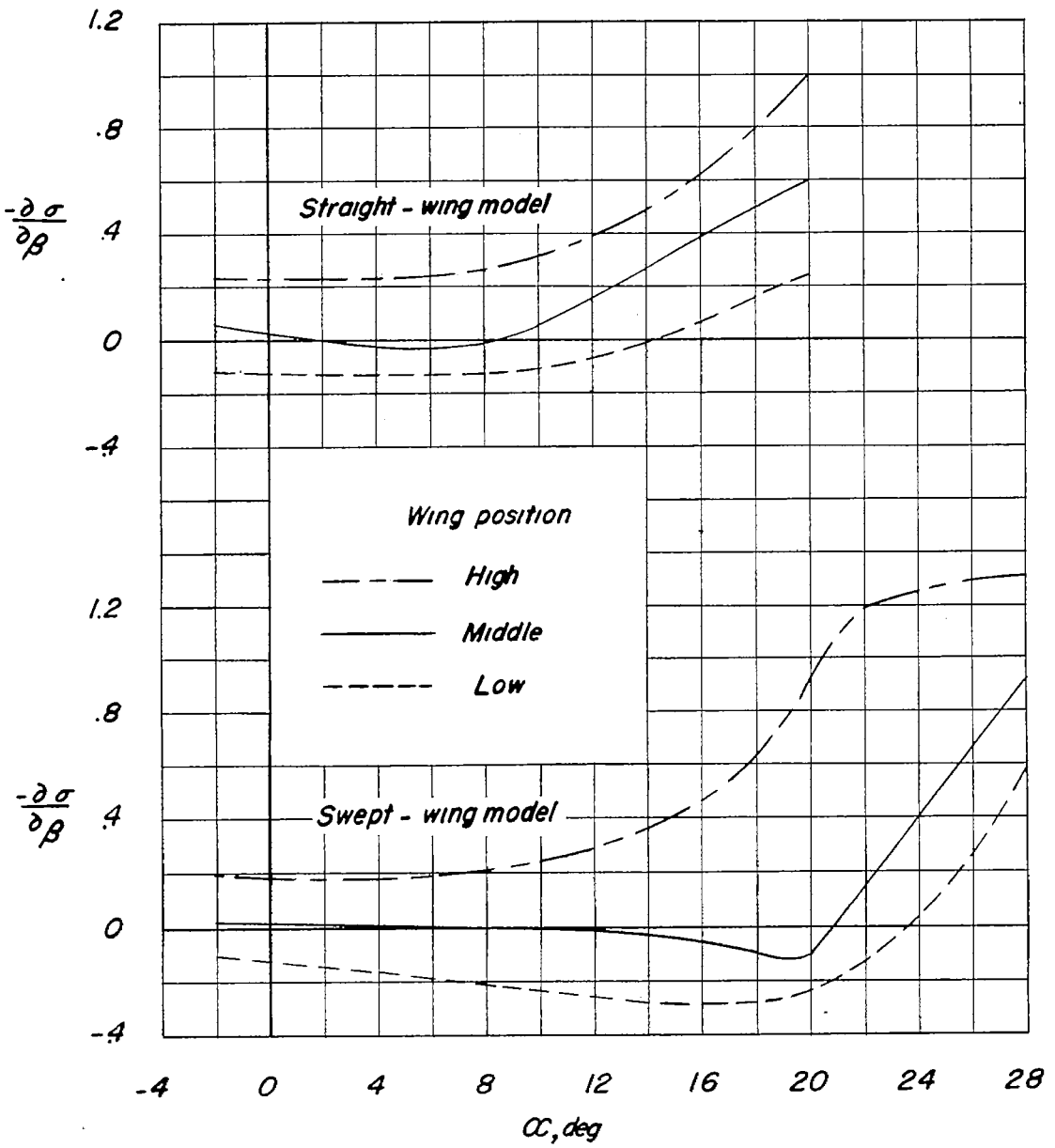

Figure 13.- The sidewash characteristics of the models with varying wing position. (Data from ref. 4.)

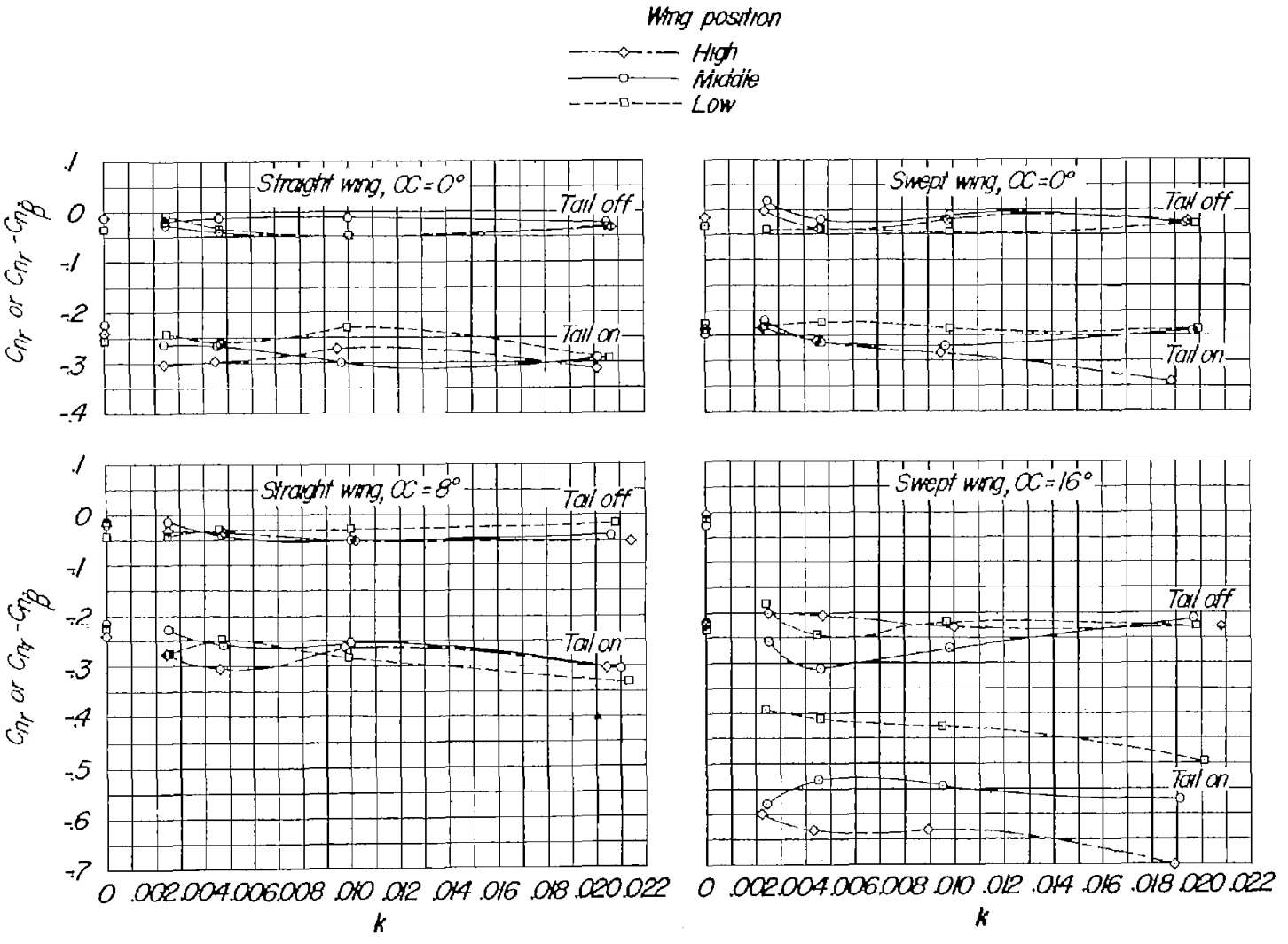

Figure 14.- The steady and oscillatory damping in yaw of the models with varying wing position for a range of reduced frequency.

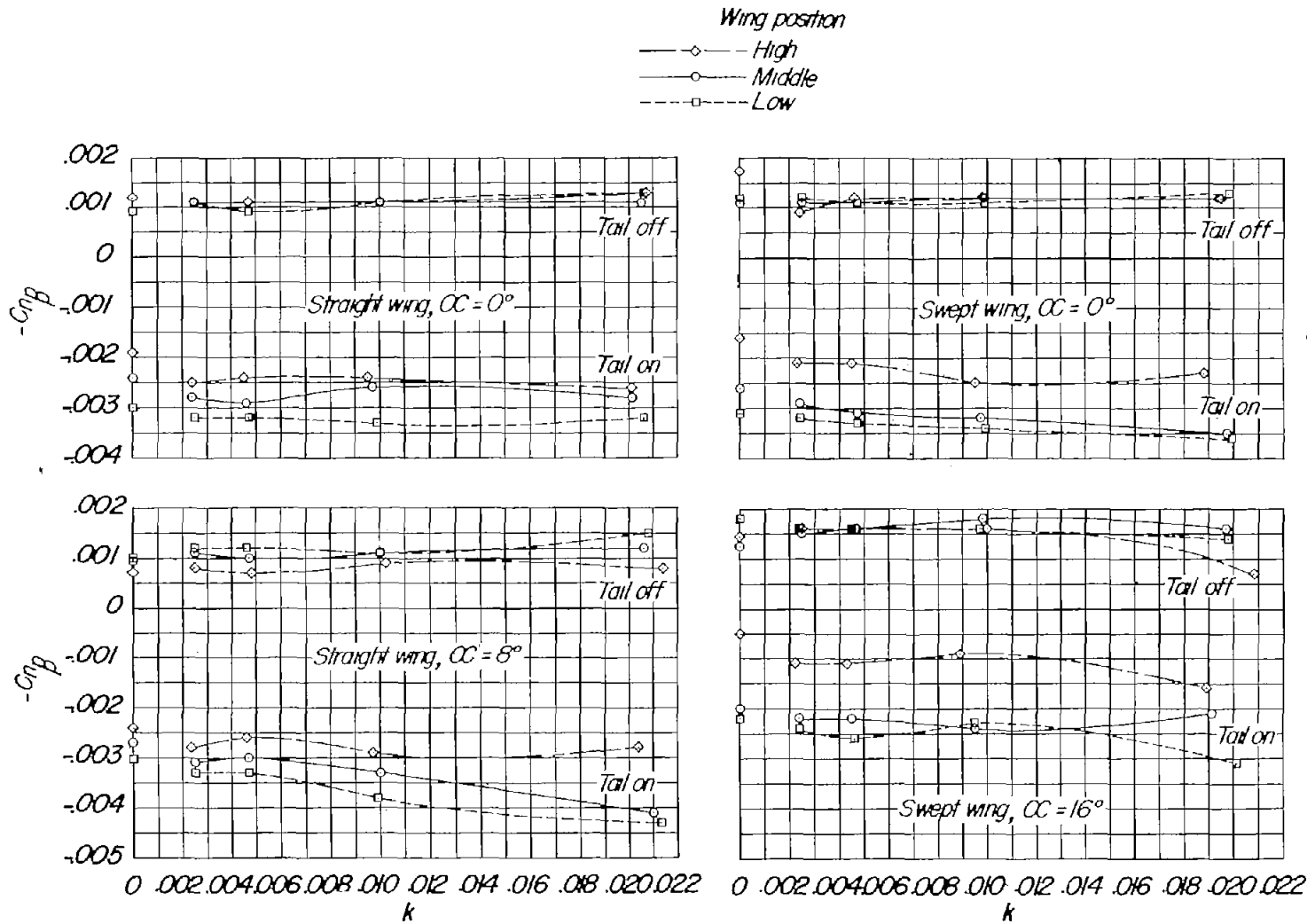

Figure 15.- The steady and oscillatory directional stability of the models with varying wing position for a range of reduced frequency.

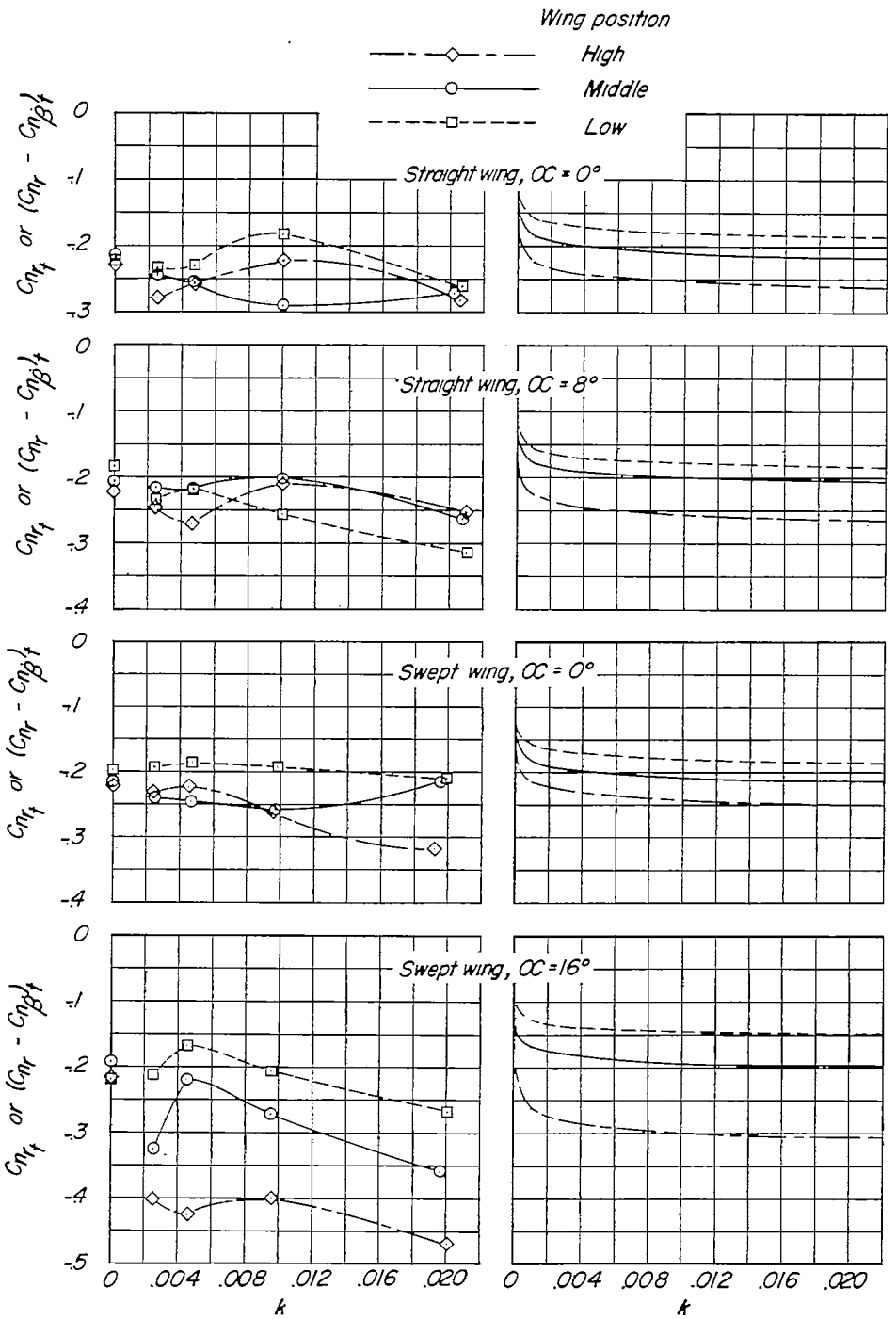

(a) Experimental. (b) Calculated.

Figure 16.- The vertical-tail increments to the damping in yaw of the models with varying wing position.

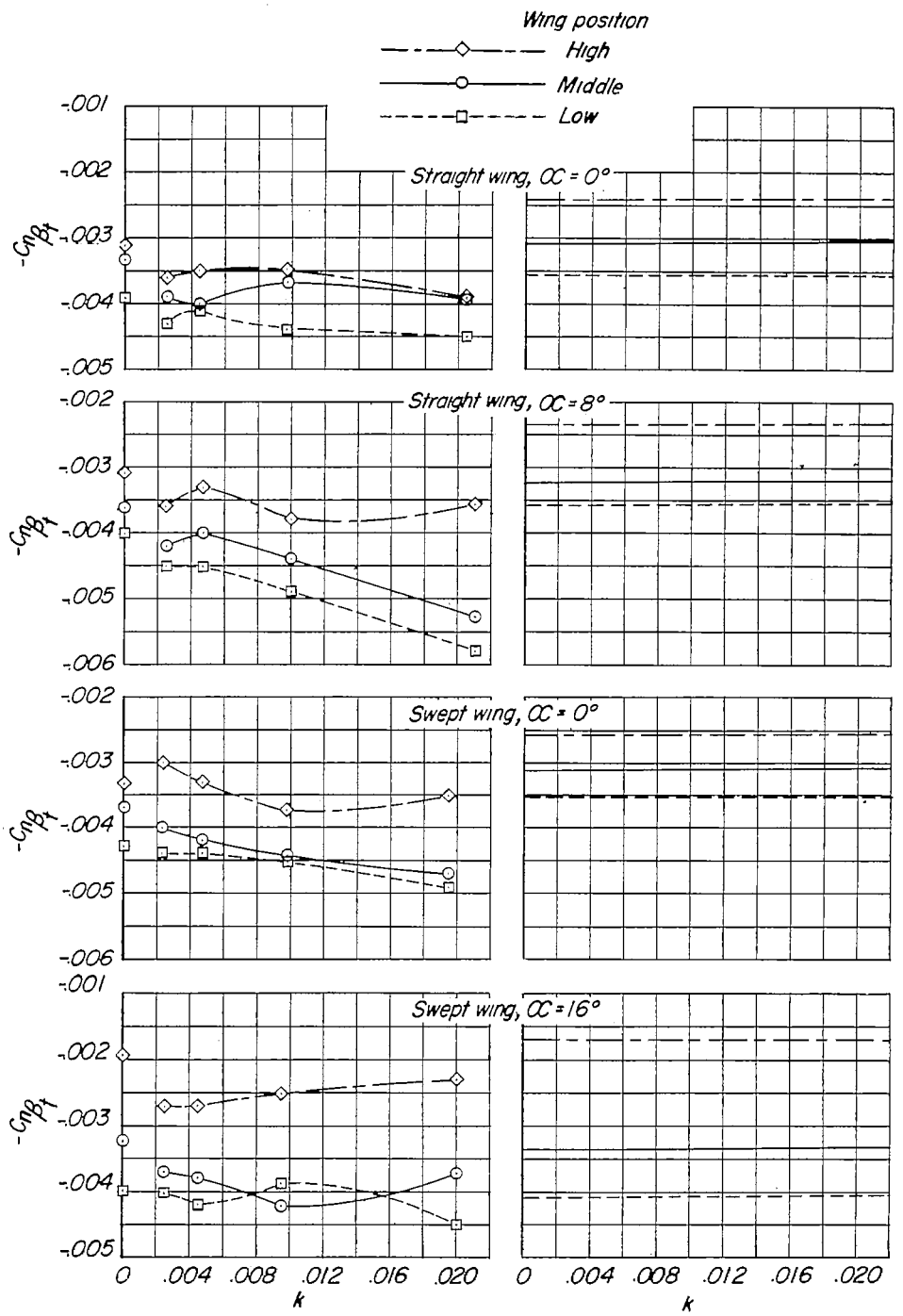

(a) Experimental. (b) Calculated.

Figure 17.- The vertical-tail increments to the directional stability of the models with varying wing positions.

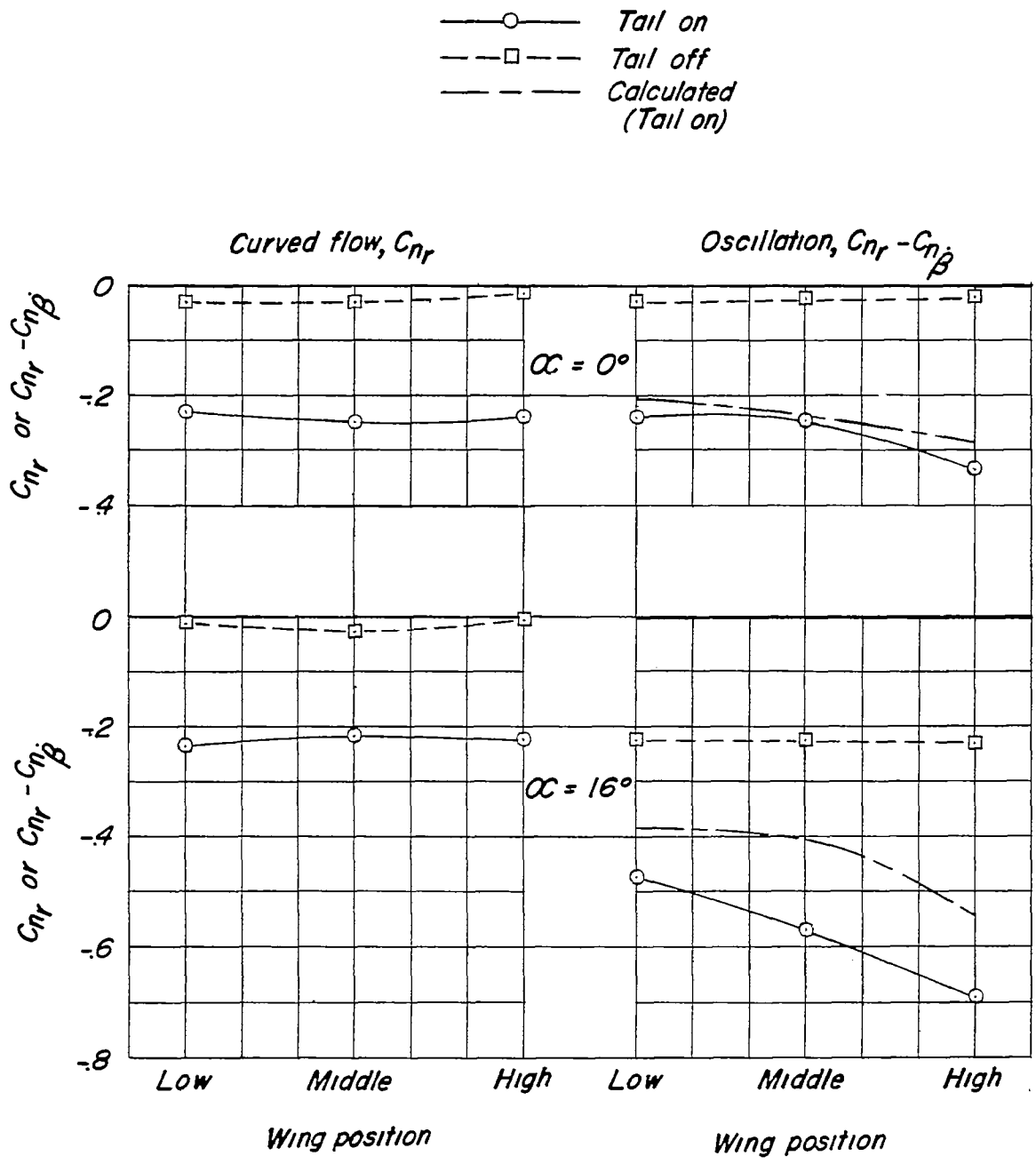

Figure 18.- The influence of wing position on the steady and oscillatory damping in yaw of the swept-wing model. k = 0.018.

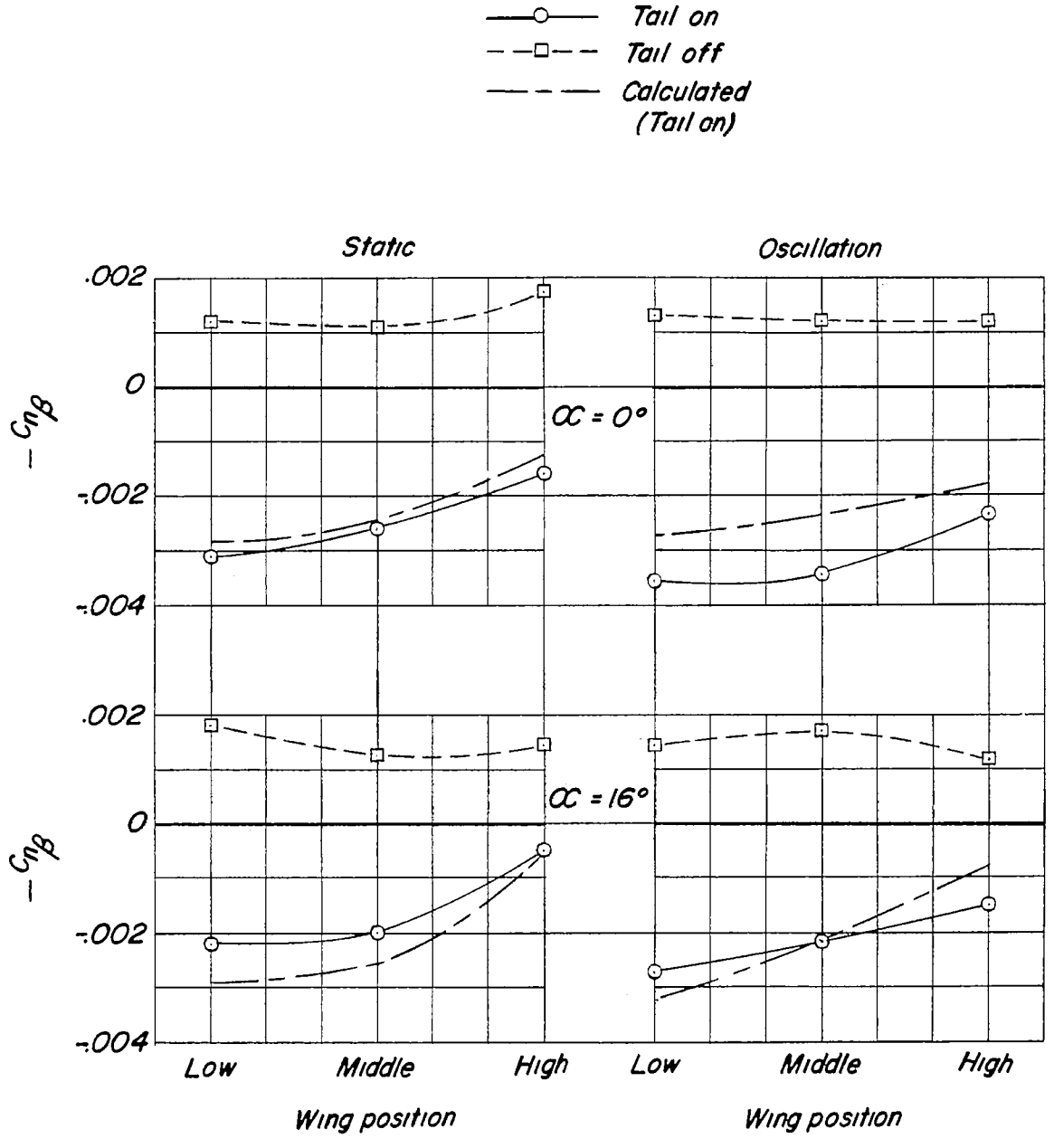

Figure 19.- The influence of wing position on the steady and oscillatory directional stability of the swept-wing model. k = 0.018.